Distorted chain sites for Co- and Fe-substituted $YBa_2Cu_3O_{7-\delta}$

F. Bridges
Department of Physics, University of California, Santa Cruz, California 95064

J. B. Boyce
Xerox Palo Alto Research Center, Palo Alto, California 94304

T. Claeson
Physics Department, Chalmers University of Technology, S-41296 Gothenberg, Sweden

T. H. Geballe
Department of Applied Physics, Stanford University, Stanford, California 94305

J. M. Tarascon
Bell Communications Research Laboratory, Red Bank, New Jersey 07701
(Received 28 December 1988)

We present x-ray-absorption fine-structure (XAFS) measurements for a series of Co- and Fe-substituted samples of $YBa_2Cu_3O_{7-\delta}$ (Y-Ba-Cu-O). Our analysis of the first- and second-neighbor environments indicates that the Co atoms primarily replace the Cu in the chain sites, the Cu(1) atoms, in Y-Ba-Cu-O, but many of these Co(1) sites and their neighboring oxygen sites are highly distorted. The first-neighbor Co-O peak consists of ~ 3.5 oxygen at 1.8 Å and ~ 1.3 oxygen at 2.4 Å, while the second-neighbor multipeak in the XAFS data is unexpectedly low in amplitude. Structure in this peak is inconsistent with a simple Gaussian broadening and indicates that several Co(1)-Ba distances exist. We propose an aggregation of the Co atoms into distorted, zigzag chains along the ⟨110⟩ directions, with some of the Co displaced off center by ~ 0.4 Å along a perpendicular ⟨110⟩ direction. This model is consistent with the second-neighbor XAFS data, provides an explanation for the tetragonal structure via twinning on a microscopic scale, and accommodates excess oxygen within the Co chains. The Fe data suggest that similar chains also exist in the Fe-substituted samples. There are, however, some differences between the local environments of the Fe and Co. The primary difference is that a small but significant number of Fe atoms occupy the Cu(2) plane sites while no appreciable number of Co atoms are found on the Cu(2) sites in the more dilute samples. Finally, near-edge measurements on the Co and Fe K-absorption edges indicate that the valence is primarily +3, but a mixture of valences exists. For Co, the edge position corresponds to a mixture of +2 and +3 valences, while Fe exists in a mixture of +2, +3, and +4 states.

I. INTRODUCTION

In nearly all the high-T_c superconductors discovered to date[1-10] (the exception being $Ba_{1-x}K_xBiO_3$),[11] planes or chains of Cu and O play a crucial role since the superconducting electrons are found in these layers. However, the nature of the pairing interaction and an explanation as to why Cu is so important are as yet unanswered questions. To probe this aspect, several groups have substitutionally replaced some of the Cu in $YBa_2Cu_3O_{7-\delta}$ (Y-Ba-Cu-O) with other atoms;[12-49] a partial list includes Fe, Co, Ni, Zn, and Mn. In each case, a relatively small concentration of the defect decreases the transition temperature T_c substantially, and for 15% substitution many systems are no longer superconducting.[12,14,28-33] The suppression of T_c occurs for both magnetic (Fe, Co, and Ni) and nonmagnetic (Zn) defects; in fact, Zn is more effective at lowering the transition temperature.[28-33] Thus, magnetic interactions are probably not the most important feature of this effect.

Another aspect of the substitutional doping of these materials is the assumption that the environment about a defect is essentially the same as the environment about a Cu atom on either the Cu(1) or Cu(2) sites (see Fig. 1 for a definition of the various sites). For example, in Mössbauer experiments,[41-49] substitutional ^{57}Fe has been used to probe the Cu environment. These measurements suggest that several different O coordinations exist about the Fe (fourfold, fivefold, and sixfold) and that two valences are present—Fe^{3+} and Fe^{4+}. The proposed environments assume that the Fe atom is located primarily at the Cu(1) site, with a small occupation of the Cu(2) site. It is important to know whether or not the substituted site is distorted to ascertain the validity and limitations of using such a probe.

In this contribution, we have used the x-ray-absorption

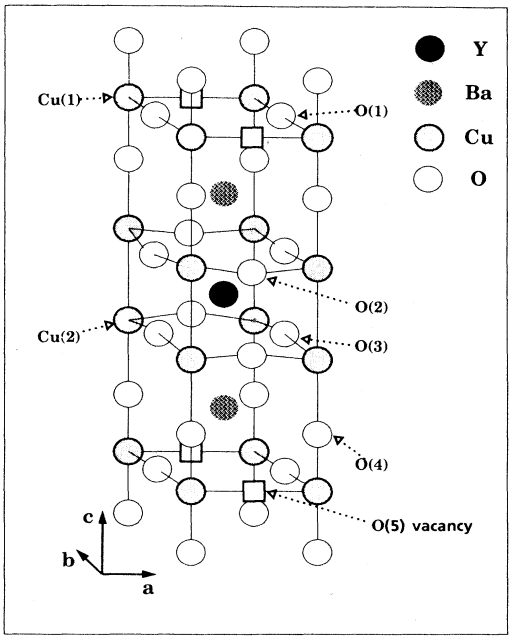

FIG. 1. The structure of $YBa_2Cu_3O_{7-\delta}$ for $\delta=0$, the fully oxygenated case ($y=7$) using the notation from Jorgensen *et al.* (Ref. 7) for the atomic sites. In the ideal case the O(5) sites are vacant. For $\delta=1$ ($y=6$), the O(1) are fully depleted and the *a* and *b* axes are equivalent.

fine-structure (XAFS) technique[50,51] to probe the local structure around Fe and Co in Y-Ba-Cu-O. Several preliminary presentations have been given previously.[52–56] We find that Co substitutes primarily at the Cu(1) site, in agreement with other investigations. Fe is also predominantly found on the Cu(1) site but some occupancy of the Cu(2) site also occurs. More importantly, we find that many of the substituted sites are significantly distorted, with some of the Co (or Fe) atoms displaced (probably along the ⟨110⟩ direction) from the position a Cu(1) atom would normally occupy. Most of our analysis focuses on the Co measurements since our data are much more extensive for this system. The Fe data appear similar to Co in both the first- and second-neighbor shell, and were analyzed using the understanding gained from our investigation of the Co systems.

The paper is organized as follows. In Sec. II we describe the samples and provide some experimental details. In Sec. III we present the XAFS data and the analysis for the near-neighbor environment about the Co atoms. Some results for the Cu near-neighbor environment are also included. The composite second-neighbor environments for Co and Cu are considered in Sec. IV and the Fe results are presented in Sec. V. The near-edge structure for the Fe and Co *K* edges in substituted Y-Ba-Cu-O and for the Cu *K* edge in undoped and Co-substituted Y-Ba-Cu-O, are discussed in Sec. VI. Finally, we compare our results with other experiments on substituted Y-Ba-Cu-O materials in Sec. VII, and summarize our conclusions in Sec. VIII.

II. SAMPLES AND EXPERIMENTAL ASPECTS

We have performed XAFS transmission experiments at the Co *K* edge in $YBa_2(Cu_{1-x}Co_x)_3O_{7-\delta}$ for $x=0.017$, 0.033, 0.067, 0.17, and 0.30, and at the Fe *K* edge in $YBa_2(Cu_{1-x}Fe_x)_3O_{7-\delta}$ for $x=0.033$, 0.10, and 0.17. In addition, we have made measurements at the Cu *K* edge for the $x=0.033$ and 0.3 Co samples, and for several normal Y-Ba-Cu-O ($x=0$ and $\delta\approx 0$) samples. The XAFS samples were prepared by brushing a fine powder of the sample onto Scotch tape. Several layers, typically 3–4 for the Cu *K* edge, were stacked to obtain a sample with a thickness of approximately two absorption lengths. Each XAFS sample was selected to be free of pinholes; an x-ray picture of each sample was taken at the synchrotron to check this selection process. For all samples several data sets were collected to check for consistency; for the lower concentration samples, many data sets were collected and averaged to improve the signal-to-noise ratio. Data were also collected for a series of reference materials including CoO, Co_3O_4, FeO, Fe_3O_4, Fe_2O_3, Cu_2O, and CuO.

The Y-Ba-Cu-O samples have been characterized using x-ray diffraction, thermogravimetric analysis, Meissner effect, and resistivity studies. The x-ray-diffraction studies show that within the resolution of these measurements (a few percent) all samples are single phase except for the $Co_{0.3}$ material. The latter showed a small amount ($<10\%$) of another phase. Excluding the $Co_{0.017}$ sample, for which the S/N of the XAFS data is poor, all the samples have a tetragonal crystal structure. The O content increases with Co or Fe substitution in general, and all the samples studied have high O concentrations. For the Co samples, $y=7-\delta$ varies from 6.92 to 7.3 while for the Fe samples y varies from 6.92 to 7.2. Further details about the characterization of these samples and an analysis of the results of measurements made using the above techniques are given in Ref. 14.

The XAFS experiments were carried out on Beamline 7-3 at the Stanford Synchrotron Radiation Laboratory (SSRL) using Si(400) monochromator crystals. A leveling feedback system was used to control the piezoelectric crystal of the monochromator to keep the incident photon flux constant;[57] for the very narrow rocking curve of the (400) crystals this feedback scheme is crucial to remain on the rocking curve over a 1.5-keV sweep in energy. Most of the experiments were made at 80 K using a liquid-nitrogen dewar or an Oxford variable-flow helium cryostat. A few measurements were taken at lower (4.2 K) and higher (300 K) temperatures.

The XAFS spectrum is extracted from the absorption data using standard procedures.[50,51] First a polynomial or spline fit to the pre-edge data is subtracted from the entire data set. Then a spline fit to the data above the absorption edge is used to remove the background from the XAFS oscillations, and the energy data converted to *k*-space data, $k\chi(k)$, using $k=[2m(E-E_0)]^{1/2}/\hbar$, where $\chi(k)$ is defined by the equation $\mu(k)=\mu_0[1+\chi(k)]$, μ_0 is the absorption at the step, E_0 is the edge position, and $\mu(k)$ is the k-dependent absorption coefficient. Finally, a fast Fourier transform is applied to obtain the complex, *r*-space data $\mathrm{FT}[k\chi(k)]$.

III. Co (AND Cu) NEAR-NEIGHBOR ENVIRONMENT

A. Data presentation

In Fig. 2 we compare the real-space Co K-edge XAFS data FT[$k\chi(k)$] for the $Co_{0.17}$ sample with the Cu K-edge data for normal Y-Ba-Cu-O. Both the amplitude and the real component of the complex Fourier transform are plotted. In each case, the k-space transform range is 3.6–11.7 $Å^{-1}$ with a Gaussian broadening of 0.5 $Å^{-1}$. The main features to note are (1) the first-neighbor environment is similar for the two atoms but the main peak for Co is shifted to lower r by roughly 0.1 Å (note that this peak in the r-space XAFS data includes a phase shift—the actual distance is about 1.8 Å), (2) there is additional weight near 2.0 Å for the Co edge, and (3) the second-neighbor peaks, in the range 2.5–4.5 Å, are considerably reduced in amplitude for the Co-edge data (see Sec. IV).

The data for all the Co samples are similar, as shown in Fig. 3, but there are differences in composition. The most striking is the changing shape and decreasing amplitude of the second-neighbor peak discussed in Sec. IV. The first-neighbor Co-O peak does decrease in height (as a result of broadening) and there is a small change of phase of the real part of FT[$k\chi(k)$] (corresponding to a small change in the splitting between the Co-O components). The first-neighbor results are qualitatively inconsistent with the predictions obtained by assuming a simple replacement of the Cu(1) by Co. The additional weight in the 1.9–2.3 Å region is quite unexpected since *no* long Cu–O bonds occur for the Cu(1) sites. A significantly shortened Co–O bond length along the chains compared to the Cu-O chain distance of 1.94 Å appears inconsistent with the fact that the lattice constant increases very slightly when Co is introduced.

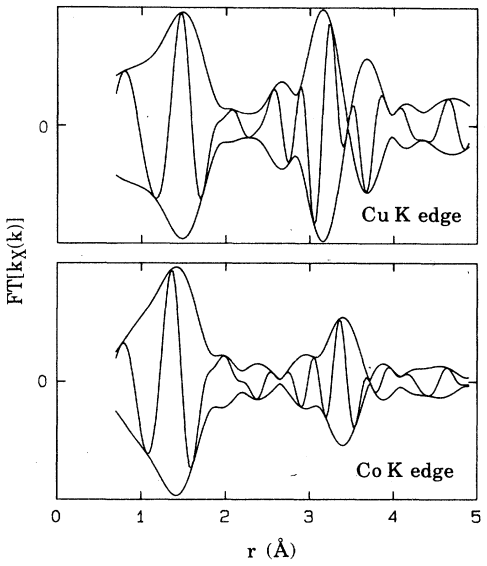

FIG. 2. A comparison of the Fourier transform of the K-edge XAFS $k\chi(k)$, to real space for Cu in Y-Ba-Cu-O with $y=6.87$ and Co in Y-Ba-Cu-O($Co_{0.17}$). The transform range is a square window from 3.6 to 11.7 $Å^{-1}$, Gaussian broadened by 0.5 $Å^{-1}$. The envelope curve is the magnitude of the complex transform (plotted as $+|\mathrm{FT}[k\chi(k)]|$ and $-|\mathrm{FT}[k\chi(k)]|$) and the oscillatory curve is the real part of the transform. The vertical scales in each case are the same, and the tic at the center of the vertical axis is the zero point. There is a shift of the XAFS peaks from the actual positions due to the phase shifts. The main Co-O peak at 1.4 Å is shifted downward by roughly 0.1 Å compared to the Cu-O peak; the second-neighbor structure is greatly reduced for the Co K edge. Note also the increased weight of the main peak and near 2.0 Å for the Co K edge.

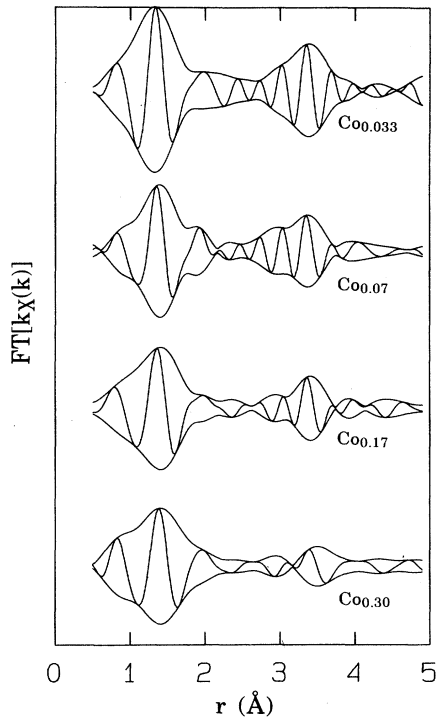

FIG. 3. The Fourier transform of the Co K-edge XAFS, $k\chi(k)$, for several Co concentrations. Note the increasing interference at 3.2 and 3.7 Å as the concentration increases.

B. Data analysis

To carry out a detailed analysis of the various peaks, we first developed a set of single-peak standards for Cu-O, Cu-Ba, and Cu-Y that provide an excellent fit to normal and O-depleted Y-Ba-Cu-O. Details of these standards are discussed in a separate paper.[58] Next we modified these standards slightly by correcting the central atom phase shifts[59] to correspond to Co or Fe. For the cases where tests were possible, e.g., CoO and Co_3O_4, the generated standards fit the experimental standards very well. In Fig. 4, we show the k-space and r-space data for the Cu-O and generated Co-O peaks for a bond length of 1.85 Å. Note that the major change in going from Cu-O to Co-O is a small, nearly constant shift of the k-space data which results in a small change in the phase shift between the real and imaginary parts in the r-space data (compare the positions of the oscillations of the real part in Fig. 4), but no change in the amplitude function.

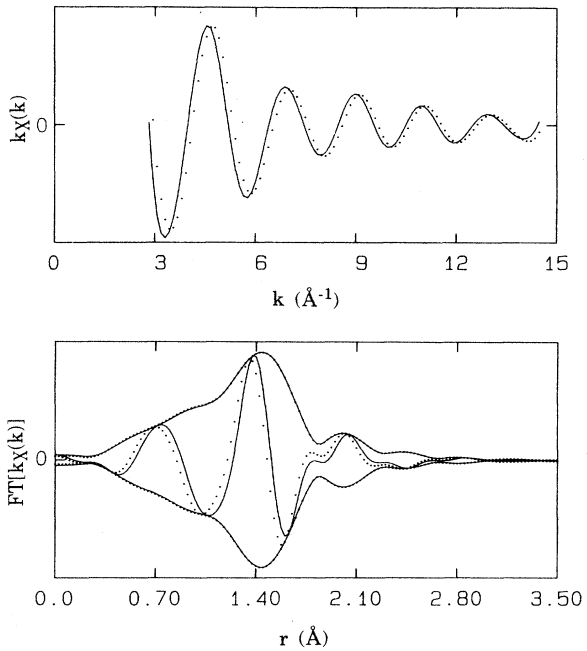

FIG. 4. A comparison of the Cu-O standard (solid line) and the Co-O standard (dotted line) generated using the central atom phase shifts of Teo and Lee. Note the nearly constant shift of the Co-O k-space data relative to the Cu-O data.

TABLE I. The room-temperature near-neighbor distances and number of neighbors around the Cu(1) and Cu(2) atoms in orthorhombic $YBa_2Cu_3O_7$ within a radius of 4 Å. The notation is from Jorgensen *et al.* (Ref. 7) (Fig. 1), and the structure for $y=7$ from Beno *et al.* (Ref. 2). The average numbers are the weighted averages, normalized to the total number of Cu atoms present. The weighted averages are used in comparisons with the XAFS results.

Cu-X pair	Number of neighbors	r (Å)	Average number	Average r (Å)
Cu(1)-O(4)	2	1.85	$\frac{2}{3}$	1.85
Cu(1)-O(1)	2	1.94		
Cu(2)-O(2)	2	1.93	$\frac{10}{3}$	1.94
Cu(2)-O(3)	2	1.96		
Cu(2)-O(4)	1	2.30	$\frac{2}{3}$	2.30
Cu(2)-O(2)	2	3.66	$\frac{8}{3}$	3.66
Cu(2)-O(3)	2	3.65		
Cu(2)-Y	4	3.20	$\frac{8}{3}$	3.20
Cu(2)-Ba	4	3.38	$\frac{8}{3}$	3.38
Cu(1)-Ba	8	3.47	$\frac{8}{3}$	3.47
Cu(2)-Cu(2)	1	3.37	$\frac{2}{3}$	3.37
Cu(2)-Cu(2)	2	3.82		
Cu(2)-Cu(2)	2	3.88	4	3.85
Cu(1)-Cu(1)	2	3.82		
Cu(1)-Cu(1)	2	3.88		

The first-neighbor Co peak was fit to a sum of Co-O standards starting with the known distances and number of O neighbors around the Cu in Y-Ba-Cu-O. Fits assuming that the Co were all on the Cu(1) sites, all on the Cu(2), or uniformly distributed on both sites were carried out. In each case the fits converged to an unexpected result—the first-neighbor shell about Co contains about 5 atoms, but with ~3.5 O at a short distance (~1.8 Å) and about ~1.3 O at a much larger distance (2.4 Å). For comparison, the weighted number of O neighbors in Y-Ba-Cu-O (see Table I) are $\frac{2}{3}$ neighbor at 1.85 Å, $\frac{10}{3}$ neighbors at 1.94 Å, and $\frac{2}{3}$ neighbor at 2.3 Å. In Table II we summarize the results of the fits to the first-neighbor peak for several samples. These results confirm the qualitative results discussed above. We note at this point that further attempts were made to decompose the short Co-O peak into two peaks as is found for the Cu-O nearest-neighbor peak in Y-Ba-Cu-O (1.80 and 1.94 Å). In each case, these fits essentially collapsed to a single peak; if two peaks exist, they are separated by ≤ 0.05 Å. The quality of the fits is very good as shown by the excellent agreement displayed in Fig. 5 between the calculated curve (with peaks at 1.81 and 2.35 Å) and the data for $x=0.07$.

To proceed with the analysis of the Co-O peak, we must first anticipate a result from the following section on the second-neighbor environment that is consistent with other investigations—that the Co substitutes primarily on the Cu(1) site. If we further assume that the Co-O(4) distances are essentially unchanged, we must then accommodate both long and short Co-O distances within the Cu(1)-O layer. In addition, because of the tetragonal structure, the nearest-neighbor planar O are no longer constrained to the chains and it is possible that some Co have 3 or 4 nearest-neighbor O within the plane containing the Cu(1) sites. We note at this point that the sum of one long plus three short Co-O distances is very close to four Cu-O distances in the tetragonal crystal. (One long plus two short distances is only a little shorter than three Cu-O distances). We return to possible models after a discussion of the second-neighbor environment.

We also investigated the nearest-neighbor environment for Cu in the highly doped $Co_{0.3}$ sample. For this material, from other investigations, most of the remaining copper should be on the Cu(2) sites, with four neighbors at about 1.95 Å and one neighbor at 2.33 Å. The XAFS first-neighbor results are in reasonably good agreement

TABLE II. Co K-edge results for the Co-O near-neighbor environment in tetragonal $YBa_2(Cu_{1-x}Co_x)_3O_{7-\delta}$.

	Peak 1		Peak 2	
Cobalt Fraction x	Number of O neighbors	Co-O distance (Å)	Number of O neighbors	Co-O distance (Å)
0.017	3.2	1.75	1.4	2.39
0.03	3.6	1.80	1.6	2.42
0.07	3.4	1.81	1.4	2.35
0.17	3.8	1.84	0.9	2.33
0.30	3.8	1.87	1.0	2.39

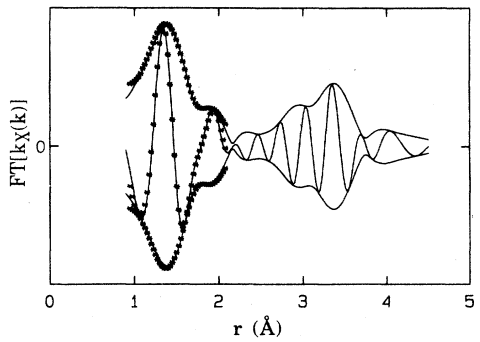

FIG. 5. A fit of the nearest-neighbor Co-O peak in the Y-Ba-Cu-O($Co_{0.07}$) sample to two Co-O standards. The solid line is the data and the dotted line the fit.

with this prediction; no short bond is observed, at 1.85 Å one neighbor is found at 2.38 Å and 4.5 neighbors are found at 1.93 Å (see Table III).

IV. Co (AND Cu) SECOND-NEIGHBOR ENVIRONMENT

A. Data presentation

The second-neighbor environment for a direct substitution of Co at the Cu(1) sites should be simpler than that for the usual mixture of Cu(1) and Cu(2) sites in normal Y-Ba-Cu-O (see Table I). The Cu(1) site has only *two* second-neighbor peaks in the range 2.5–4.0 Å; 8 Ba neighbors at 3.47 Å, and 4 Cu neighbors in the range 3.82–3.88 Å. The Cu(2) site is a more complicated environment, having 4 Ba neighbors at 3.38 Å, 4 Y neighbors at 3.2 Å, 1 Cu neigbor at 3.37 Å, and 4 Cu neighbors in the range 3.82–3.88 Å. The resultant weighted averages for these two sites in Y-Ba-Cu-O, normalized to the total number of Cu atoms are given in Table I. The important points to emphasize are that the total Cu-Ba amplitude for the Cu(1) site is *50% larger* than the total weighted Cu-Ba amplitude in Y-Ba-Cu-O, and only two main peaks contribute to the undistorted Cu(1) second-neighbor shell. Such a Cu(1) environment should yield a large and well-defined second-neighbor shell between 2.6 and 3.9 Å with an amplitude that is larger than observed for the Cu *K*-edge data because less interference should occur with fewer peaks. The experimental reality is quite different for the Co *K*-edge data (see Figs. 2 and 3); the second-neighbor peak is small and cannot be fit by such a simple composition.

B. Data analysis

In our initial attempts to fit the second-neighbor Co data we used two peaks, corresponding to the expected Cu−Ba and Cu−Cu(Co) bonds for the Cu(1) site. Even with significant broadening the fit to the data was very poor and the number of Ba neighbors was far too low. Adding a Co(2)-Y peak at 3.2 Å and a small Co(2)-Ba peak at 3.4 Å to include the possibility of a partial Cu(2) site occupancy for Co did not improve the fit greatly. In such fits, the Co-Y amplitude is always reduced to values corresponding to less than 15% of the Co on Cu(2) site. The reduced second-shell amplitude is indicative of significant disorder for the Co second-neighbor-atom distances, but it is clearly not a Gaussian broadening of the expected peaks. Structure in the Fourier-transformed *r*-space data suggests a strong interference between several peaks, somewhat similar to the effect observed in O-depleted Y-Ba-Cu-O, in which the net Cu-Ba peak is greatly reduced.[58]

Before discussing the Co second neighbors in more detail, it is instructive to first consider the question: is the

TABLE III. The Cu near-neighbor distances and weighted number of neighbors around the Cu(1) and Cu(2) sites in tetragonal $YBa_2(Cu_{0.7}Co_{0.3})_3O_{7-\delta}$. The number of neighbors is calculated assuming (1) that the Co is entirely on the Cu(1) site and (2) that 11% of the Co is on the Cu(2) site. The weighted number includes the fractional occupancy and normalizes to the total amount of Cu. The Cu-Cu peak includes forward scattering from an intervening O. This increases the amplitude and changes the phase shift such that the apparent distance is about 0.1 Å longer.

	Diffraction distance no Co on Cu(2)		Diffraction distance 11% Co on Cu(2)		EXAFS	
Cu-*X* pair	Weighted number of *X* neighbors	Cu-*X* distance (Å)	Weighted number of *X* neighbors	Cu-*X* distance (Å)	Weighted number of *X* neighbors	Cu-*X* distance (Å)
Cu(1)-O(4)	0.1	1.85	0.19	1.85	. . .	. . .
Cu(1)-O(1)	0.1	1.94	0.19	1.94	. . .	. . .
Cu(2)-O(2)	3.8	1.94	3.62	1.94	4.5	1.93
Cu(2)-O(4)	0.95	2.33	0.90	2.33	1	2.38
Cu(2)-Y	3.8	3.19	3.62	3.19	3.5	3.20
Cu(2)-Ba	3.8	3.41	3.62	3.41	3.8	3.43
Cu(1)-Ba	0.4	3.52	0.8	3.52	0.8	3.55
Cu(2)-Cu(2)	3.8	3.89	3.62	3.89	[6]	[3.99]
Cu(1)-Cu(1)	0.19	3.89	0.38	3.89	. . .	. . .

Co-Ba second-neighbor peak smeared out because the Ba atoms are highly disordered? The answer, even for the highly doped $Co_{0.3}$ sample, is no, based on the Cu K-edge second-neighbor results for this sample. Unlike the Co second-neighbor peak, the Cu second-neighbor peak for the $Co_{0.3}$ sample is quite large and rather similar to normal Y-Ba-Cu-O as shown in Fig. 6. We fit the second-neighbor multipeak structure in FT$[k\chi(k)]$ from $r=2.5$ to 3.8 Å to a Cu(2)-Y, a Cu(2)-Ba, a Cu(1)-Ba, and a Cu-Cu standard, with constraints on the relative amplitudes corresponding to various percentages of Co on the Cu(2) site. A small Cu(1)-Ba peak is expected, even if Co substitutes only on the Cu(1) site, because a 30% Co substitution leaves 10% of the Cu(1) sites occupied by Cu. If some of the Co goes into the Cu(2) plane, the percentage of Cu on Cu(1) sites will increase. We obtained a very good fit (see Fig. 7) with the parameters given in Table III. If most of the Co are on the Cu(1) sites, and, therefore most of the remaining Cu are on the Cu(2) sites, we expect the average number of Y neighbors about a Cu to increase from 2.67 (for Y-Ba-Cu-O) to nearly 4 (compare Tables I and III), and the two Cu-Ba peaks to have quite different amplitudes. Within a 13% uncertainty in the number of first- and second-nearest neighbors, the amplitudes of the two O peaks, the two Ba peaks, and the Y peak are consistent with a Co site distribution of $\sim 11\%$ of the Co on Cu(2) sites and $\sim 89\%$ on Cu(1) sites in this highly doped sample. However, a reasonable fit is possible with 5% to 20% on the Co on Cu(2) sites. (Beyond these limits, the quality of fit parameter (a weighted χ^2 parameter) increases rapidly; in addition, the amplitudes become too high or too low and the positions of the peaks begin to shift). We also note that the Cu−Ba bond lengths agree very well with those measured by neutron diffraction for a

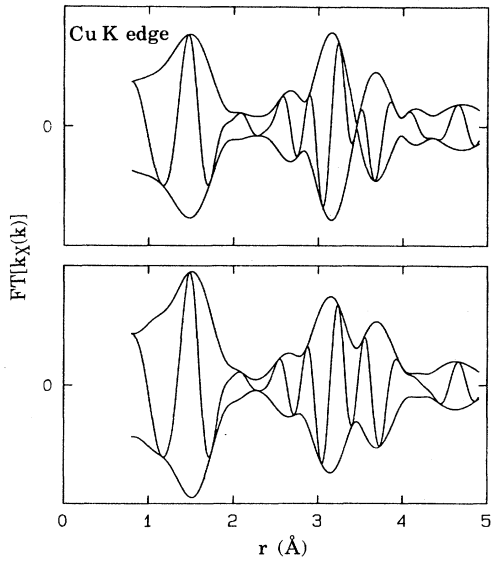

FIG. 6. The Fourier transform of the Cu K-edge XAFS, $k\chi(k)$, for normal Y-Ba-Cu-O and the Y-Ba-Cu-O($Co_{0.30}$) samples. In the Co-doped sample, the Cu-O peak is slightly larger and the second-neighbor multipeak is quite similar to the corresponding peak in Y-Ba-Cu-O.

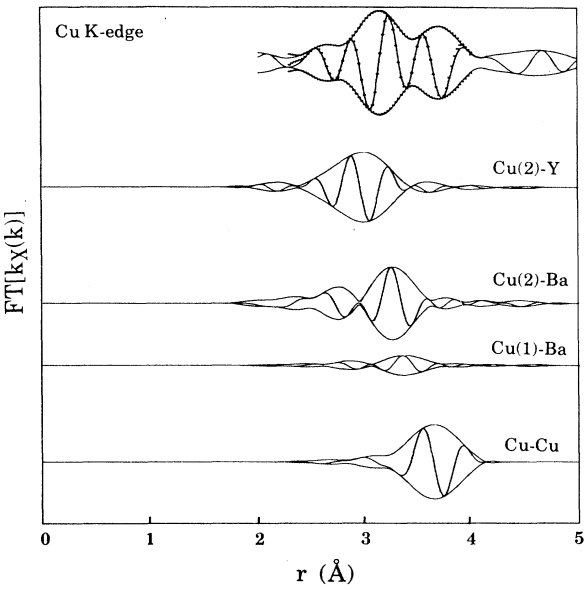

FIG. 7. A fit of the second-neighbor peak in FT$[k\chi(k)]$ of the Cu K-edge data for the Y-Ba-Cu-O($Co_{0.30}$) sample. The upper curve shows the data (solid curve) and the resultant fit (dotted curve). The lower curves are the four component Cu-X peaks that make up the second-neighbor fit (see Table III).

$Co_{0.27}$ sample[60] and more importantly, that the Cu-Ba peaks are only slightly broadened. Together, these results indicate that the Ba atoms, as determined from the Cu(2) planes, are well ordered and at their expected positions.

The second-neighbor Cu peak in this fit is about 0.1 Å longer than expected from the crystal structure. This is the result of forward scattering from intervening O atoms which adds an additional phase shift; a similar apparent shift in the position of this Cu-Cu peak is also observed in the undoped samples.[58]

We now consider the Co second-neighbor environment. To achieve the large reduction in the observed Co-Ba peak amplitude without any disorder on the Ba sites, requires that some of the Co must be displaced a large distance (≥ 0.3 Å) from the normal Cu(1) sites. We do not believe that the Co are on some other site for two reasons; first, the fits to the Cu K-edge data for both the first- and second-neighbor peaks of the $Co_{0.3}$ sample clearly indicate that few of the Cu atoms are on Cu(1) sites [this implies that the Cu(1) sites are occupied by Co] and second, we can fit the Co second-neighbor multipeak structure quite well with the above assumption that some of the Co are displaced.

XAFS investigations alone cannot give the positions of the second neighbors in a complicated environment but those measurements can provide a test of various hypotheses. To motivate and constrain possible models we make use of the following.

(a) For all the samples analyzed in detail, the crystal structure is tetragonal.[14] This means that when Co atoms are added to the plane containing the Cu(1) site, some oxygen atoms occupy the O(5) sites (shown as vacancies in Fig. 1) between the original Cu(1)-O(1) chains, which is

consistent with the increased O content in the Co-substituted samples.[14,21]

(b) Bordet *et al.*[21] observed streaks in their electron-diffraction patterns for low-concentration Fe-substituted samples. They interpreted this result as evidence for chains of Fe atoms along the ⟨110⟩ direction. Since the Fe and Co data are quite similar (see Sec. VI) we also assume ⟨110⟩ chains for the Co atoms.

(c) As discussed above, most of the Co(1)−O bonds are much shorter than the normal Cu(1)−O(1) distance, while a small but significant fraction of the Co−O bonds are much longer. A combination of both long and short Co−O bonds must be found in the Cu(1)-O plane such that the average lattice constant in the plane is essentially unchanged as observed in diffraction.

(d) We assume for the lower-concentration samples that the amount of Co on the Cu(2) sites is negligible.

(e) Lastly, we assume that the Co(1) atoms are not displaced along the *c* axis [the peak for the Cu−O(4) bond in the $Co_{0.3}$ sample has the expected position and amplitude].

First, consider one isolated Co atom. If it substitutionally replaces Cu(1) in the Cu−O chains the Cu(1)−O bonds would have to be stretched by 0.15 Å to allow the observed, very short Co−O distance. This we feel is not reasonable. However, if one of the chain O atoms flips to the vacant O(5) position between the chains as shown in Fig. 8(a), and if the Co moves off-center ($\sqrt{2}\times 0.15$ Å) along a ⟨110⟩ direction, then the short Co−O bonds are easily accommodated without a significant distortion of the Cu environment. Including the two *c*-axis O(4) atoms, this arrangement leads to a distorted tetrahedron of O about the Co. It does not, however, provide an explanation for the long Co−O bonds observed, nor account for the increased O content in the Co-substituted samples. Further, second-neighbor fits using the Co−Ba distances predicted from this displacement are poor; an even *larger* Co off-center displacement is required. We also point out that even at a 90° twinning boundary, the long Co−O bonds cannot be incorporated, unless the neighboring Cu−O bond lengths can be significantly shortened. These results indicate that in the samples studied, a majority of the Co atoms are not isolated atom defects.

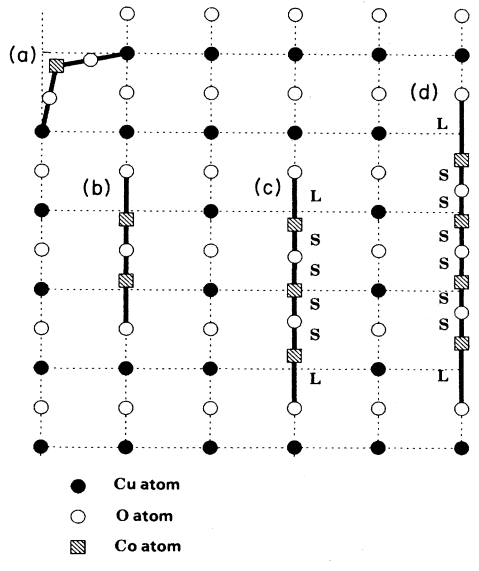

FIG. 8. Possible local structure for isolated or small clumps of Co in the Cu(1) plane. The top (a) shows an isolated Co with short Co−O bonds; (b), (c), and (d) show clumps of Co containing 2, 3, or 4 Co atoms.

Next we consider small clumps of atoms. First, pairs of Co as shown in Fig. 8(b), would allow some short Co−O bonds but would also require an intermediate Co−O distance that is not observed. A triplet of Co atoms, Fig. 8(c), along a chain permits a combination of two short and one long bond that is close to the observed value (the long bond is still a little short) for three Cu(1)−O(1) bonds. Four Co atoms in a row [Fig. 8(d)] gives a combination of one long bond and three short bonds that exactly fits within the Y-Ba-Cu-O lattice.

To obtain the tetragonal structure and also generate the ⟨110⟩ chains suggested by the diffraction measurements for the low concentration samples, we combine three-atom segments [Fig. 8(c)] with a ⟨110⟩ displacement of the end Co atoms to obtain a chain of Co−O bonds through the material as shown in Fig. 9(a). We show the Co-O-Co structure as being colinear, but it is possible that the O(1) atoms are displaced away from the line joining the Co atoms. The Co-O-Co zigzag chain can provide a twinning boundary on a microscopic scale [as shown in Fig. 9(a)] and thus lead to a macroscopic tetragonal structure, even at very low Co concentrations if the Co-O-Co chains are long enough. A more complicated double-chain version is shown in Fig. 9(b) with the Co-O-Co chain again forming a twinning boundary. Assuming the *c* axis O(4) sites are occupied, these segmented chains have either a fourfold or sixfold coordination of O about a Co atom. It is quite likely that vacancies at the O(4), O(1), or O(5) positions would provide a number of fivefold coordinated Co as well. Finally, Fig. 9(c) shows a zigzag chain formed from four-atom segments; in this case we have retained the original Cu-O chains on either side of the zigzag chain, but a twinning boundary is also possible.

For the high-concentration samples ($Co_{0.17}$ and $Co_{0.3}$) where a large fraction of the Cu(1) sites are occupied by Co, a simple, isolated zigzag chain no longer makes sense. The amplitude of the second-shell XAFS data for these samples is smaller than for the lower concentration samples, suggesting even more destructive interference. We note that there are several ways in which distorted arrays of Co atoms can be formed on a two-dimensional lattice. First the double chain of Fig. 9(b), plus a ⟨110⟩ row of on-center Co atoms on either side, can cover all the sites. However, several square supercells (composed of long and short bonds in 3×3 or 5×5 Co arrays) can also be constructed that are commensurate with the tetragonal structure observed in diffraction measurements.

The zigzag chain models shown in Fig. 9 result in specific predictions for the multipeak second-neighbor Co−Ba and Co−Cu(Co) environment. Assuming the short Co(1)−O bonds are 1.80 Å, the number of Ba and

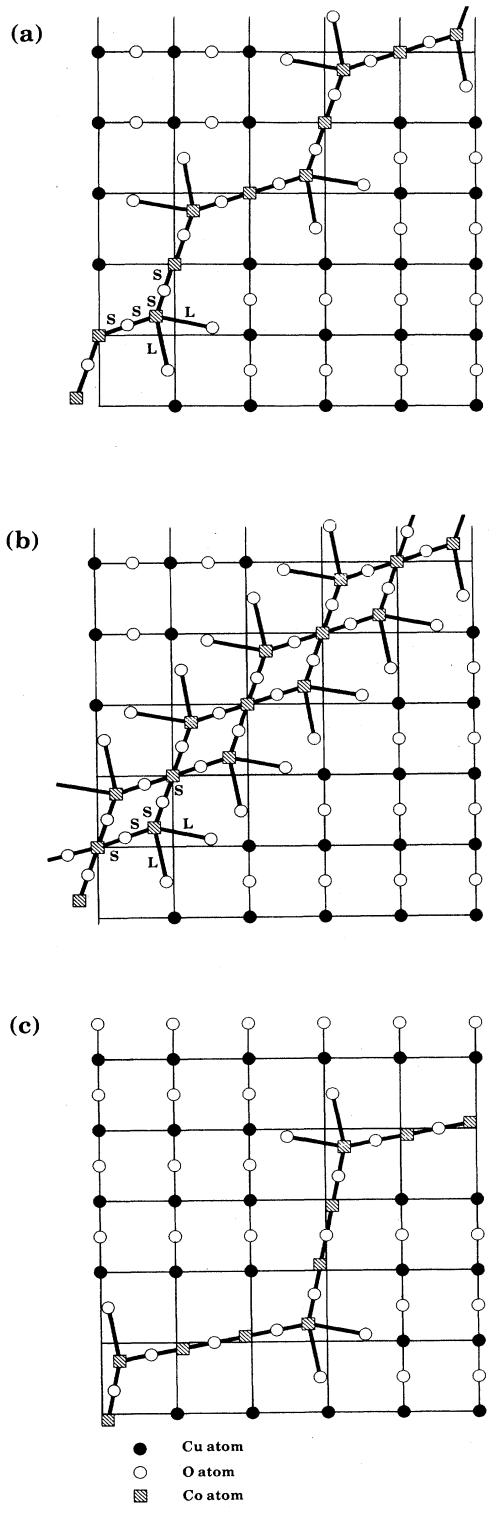

FIG. 9. Two 3-Co-atom-segment chains are shown in (a) and (b), that are consistent with (i) long and short Co−O bonds in the Cu(1) plane, (ii) the tetragonal structure [in (a) and (b), the zigzag Co chain forms a microscopic twinning boundary] and (iii) the electron-diffraction results that suggest ⟨110⟩ oriented Fe [and we propose also Co] chains. A 4-Co-atom-segment chain is illustrated in (c).

Cu (or Co) neighbors and the corresponding bond lengths are easily calculated. Note that for a ⟨110⟩ displacement of the Co by Δr_1, four of the Co−Ba distances are essentially unchanged, two are lengthened by $\delta_1 = (2/\sqrt{6})\Delta r_1$, and two are shortened by δ_1. Similarly, for a ⟨100⟩ displacement of the Co by Δr_2, four Co-Ba distances are shortened and four are lengthened by $\delta_2 = \Delta r_2/\sqrt{3}$. Multipeak fits were carried out with tight constraints on the range of the parameters—typically, 0.1 Å for the distances and 30% for the amplitudes—using the calculated results as starting parameters. Several features emerge in these fits. First a reduced amplitude peak, very close to the expected Cu(1)−Ba distance, is always present indicating some undisplaced or ⟨110⟩ displaced Co atoms. ⟨100⟩ displaced atoms would not contribute to this peak. Second, small Co displacements, such that the Co−Ba distances differ by less than 0.2 Å, are not consistent with the data; the fits always tend to increase the displacement. The most consistent fits require at least three Co-Ba peaks, one distance of 3.56 Å and the other two distances displaced symmetrically about this central distance by ±0.3 Å.

In Table IV, we compare the predictions from the 3-Co-atom single- and double-chain models (Fig. 9) to the corresponding fit results. These predictions are very similar in that the position of four of the peaks are identical. For the single-chain model, in addition to the above constraints on the range of the parameters, we set the amplitudes of the long and short Co−Ba bond peaks equal. For

TABLE IV. The second-neighbor environment for the single and double chains shown in Fig. 9 for bond lengths between 3.0 and 4.0 Å. N is the weighted number of neighbors. Fits to the low-concentration data using the predicted values as starting parameters are shown for two cases. For these fits, the parameters r and N were first constrained—$\Delta r = \pm 0.1$ Å and $\Delta N = \pm 30\%$. For the single-chain model, the long and short Co-Ba bond amplitudes were kept equal and the constraints relaxed. For the double-chain model, the three Co-Ba bonds were constrained to be in the ratio 1:4:1 and the amplitude for the Co(1)-Co(1) bond was fixed. In each case there are additional Cu neighbors at 4.15 Å and above.

Co-X pair	Predicted double chain N	r (Å)	Fit $Co_{0.033}$ N	r (Å)	Fit $Co_{0.067}$ N	r (Å)
	1.33	3.25	1.6	3.26	1.7	3.24
Co(1)-Ba	5.33	3.55	6.7	3.57	6.8	3.55
	1.33	3.89	1.6	3.87	1.7	3.84
Co(1)-Co(1)	2.67	3.55	2.67	3.52	2.67	3.56
Co(1)-Cu(1)	. . .	. . .	. . .	. . .	. . .	. . .

Co-X pair	Predicted single chain N	r (Å)	Fit $Co_{0.033}$ N	r (Å)	Fit $Co_{0.067}$ N	r (Å)
	1.0	3.25	1.6	3.26	1.4	3.24
Co(1)-Ba	6.0	3.55	3.6	3.58	3.8	3.56
	1.0	3.89	1.6	3.89	1.4	3.87
Co(1)-Co(1)	2	3.55	0.7	3.53	1.2	3.54
Co(1)-Cu(1)	1	3.85	1.4	3.90	0.5	3.81

the double-chain model, only one Co−Co distance occurs within 4.0 Å. In this case we constrained the number of Co−Ba neighbors in the ratio 1:4:1 and kept the number of Co−Co neighbors constant at 2.67 (see Table IV). The quality of the fit (a weighted percent error) is good in both cases; 0.3% and 0.6%, respectively, for the single-chain fits to the $Co_{0.033}$ and $Co_{0.067}$ samples and 1.1 and 0.9%, respectively, for the highly constrained double-chain fits. The resulting fit to the data and the separate Co−Ba and Co−Co/Cu components are displayed in Fig. 10 for the single chain case. Clearly a good fit can be obtained that is in reasonable agreement with the predictions. The constrained, double-chain model fit, requires a broadening of the Co−Ba central peak ($\Delta\sigma^2=0.017$ Å^2) and the Co-Co peak ($\Delta\sigma^2=0.01$ Å^2). The fit using the four-Co-atom single chain [Fig. 9(c)] is only slightly better, even though this model has five Co−Ba distances. The point here is not that we have found a specific model, but that displacements of the Co atoms can account for both the nearest-neighbor O peak—the combination of long and short bonds—as well as the reduced amplitude of the multipeak, second shell of neighbors for the low Co concentations. It is quite likely that several types of chains could coexist, making a unique assignment impossible.

Finally, we note that the multicomponent fits to the second-neighbor peak for the higher concentration samples, $Co_{0.17}$ and $Co_{0.30}$, are much poorer (the weighted quality of fit parameter increases by more than a factor of 5) although the signal-to-noise ratio of the k-space data for these samples is *higher*. These fits were again carried out with tight constraints on the range of the parameters, using the calculated results from the chain models as starting parameters. The poor quality of fit is consistent with the fact that for high concentrations, such that a large fraction of the Cu(1) plane has been substituted, it no longer makes sense to talk about isolated chains. Part of the problem is also the result of a small fraction of the Co residing on Cu(2) sites, which requires additional Co−Y and Co−Ba peaks. Although as discussed above, there are several structures composed of long and short bonds that are commensurate with the tetragonal structure, the large number of Co−X peaks required to describe them [plus the peaks needed for the Co atoms on the Cu(2) sites], makes a test infeasible.

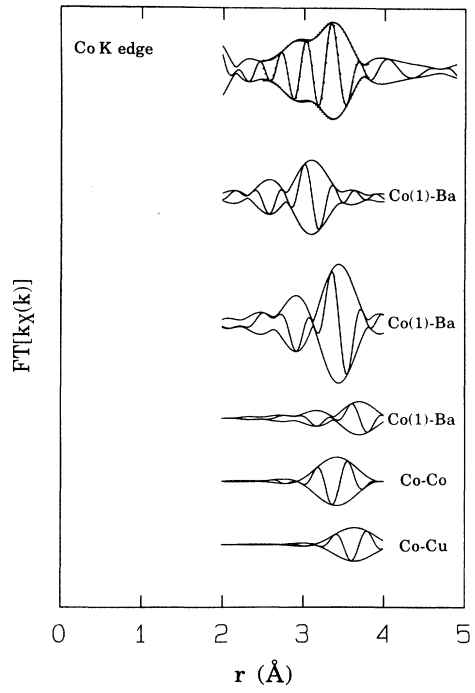

FIG. 10. The fit to the second-neighbor shell of FT[$k\chi(k)$] for the Co K-edge XAFS of the Y-Ba-Cu-O($Co_{0.07}$) sample. The upper curve is the data (solid curve) and the resultant fit (dotted curve). The lower curves are the individual Co-X contributions due to the neighboring X atoms that make up the second-neighbor fit; we assume some ⟨110⟩ displaced Co atoms as occur in the single 3-Co-atom-segment chains shown in Fig. 9(a).

V. Fe ENVIRONMENT

The XAFS results for the Fe-substituted samples are qualitatively similar to the Co results discussed above, as shown in Fig. 11, where we compare the K-edge r-space data FT[$k\chi(k)$] for Y-Ba-Cu-O($Fe_{0.10}$) and Y-Ba-Cu-O($Co_{0.17}$). Less data was collected for the Fe-substituted samples and the signal-to-noise ratio is not as good as for the Co-doped materials; only the Y-Ba-Cu-O($Fe_{0.10}$) and

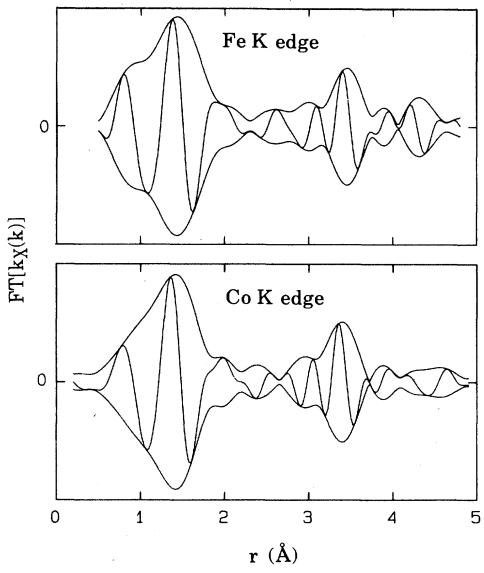

FIG. 11. A comparison of the FT[$k\chi(k)$] for the Fe K edge of Y-Ba-Cu-O($Fe_{0.10}$) and the Co K edge of Y-Ba-Cu-O($Co_{0.17}$). Qualitatively, the first- and second-neighbor peaks, from 1.0 to 4.0 Å, are similar, suggesting nearly the same local environments for Co and Fe. Quantitative fits to the first and second peaks indicate that ~20% of the Fe may be on the Cu(2) site for the higher-doped samples; in particular, an Fe-Y contribution is needed in the second-neighbor peak. In addition, the main Fe-O bond is 0.05 Å longer than the main Co-O bond in the Co-doped sample.

Y-Ba-Cu-O($Fe_{0.17}$) samples were analyzed in detail for both the first- and second-neighbor environments. For each sample, the Fe first-neighbor peak is well defined while the second-neighbor multipeak has a low amplitude and exhibits structure similar to the Co samples. This again suggests a distorted environment for the Fe atoms in Y-Ba-Cu-O. The detailed analysis is, however, not as simple. If we assume a substitution on an undistorted Cu(1) chain site, we obtain at most a fair fit to the Fe-O first-neighbor peak with roughly two neighbors at $r = 1.83$ Å and two neighbors at 1.93 Å. The major problem is that the phase in the real and imaginary parts of the fit to FT$[k\chi(k)]$ does not agree well with the data for either sample. If instead we assume a distortion, similar to that found for the Co-substituted samples discussed above, then better fits are obtained—the fit phase matches the data very well and for the Y-Ba-Cu-O($Fe_{0.10}$) sample the goodness of fit parameter decreases by a factor of 6. These fits again require long and short bonds; 3.5 to 4 neighbors at 1.88 Å and ~1.5 neighbors at 2.36 Å.

The lowest concentration sample $Fe_{0.033}$, is the most similar to Co with 4.2 neighbors at 1.84 Å and 1 neighbor at 2.4 Å. For the higher-concentration samples, the main, low-r part of the O peak can be fit equally well by 4 neighbors at 1.88 Å or 2.5 neighbors at 1.85 Å plus 1.5 neighbors at 1.93 Å, within the signal-to-noise ratio. Either of these results is again incompatible with a simple substitution on undistorted sites.

Similarities also exist for the second shell of neighbors, but multipeak fits, assuming that Fe occupies only distorted Cu(1) sites, similar to the Co case above, do not fit the data very well. The main Fe-Ba component is near 3.5 Å, consistent with the longer Fe(1)-Ba distance. Adding Fe-Y and Fe(2)-Ba peaks, at the distances necessary to represent some occupation of the Cu(2) sites, to the distorted Cu(1) site model does yield an excellent fit for ~20% of the Fe on the Cu(2) sites. Unfortunately, the number of parameters is then too large, even with the many constraints we have imposed, to place much significance on the specific values obtained. However, there is clearly no evidence for a large Fe-Y peak as would be found for an undistorted Cu(2) site occupation. Consequently, our results suggest that the Fe is primarily on the Cu(1) site and that the small Fe K-edge second-neighbor multipeak is again the result of Fe disorder on the Cu(1) sites. We note also that x-ray and neutron-diffraction data indicate a considerable amount of disorder in the Cu(1)-O(1) plane,[36,61] consistent with the off-center model proposed here.

VI. NEAR-EDGE STRUCTURE

Finally, we present a brief qualitative discussion of the near-edge structure at the K edge of the Co and Fe-doped Y-Ba-Cu-O samples. We compare the edge positions and the structure with several oxide reference materials in Figs. 12 and 13. All positions are measured relative to Co or Fe foil-edge standard data, collected at the same time using a third transmission detector. CoO and FeO have a formal valence of +2, Fe_2O_3 has a valence of +3 while

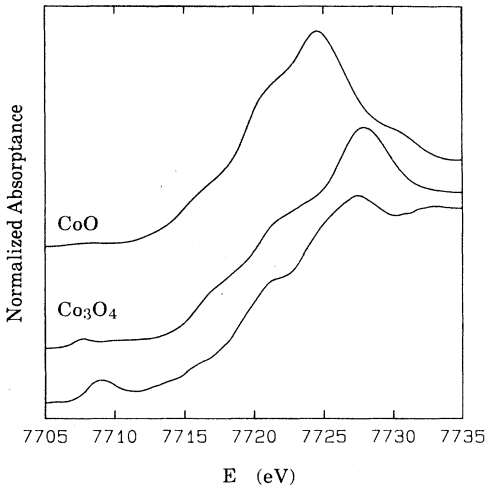

FIG. 12. The Co near-edge spectra of (from top to bottom) CoO, Co_3O_4, and Y-Ba-Cu-O($Co_{0.17}$). The vertical scale for each curve is normalized to give the same step height. The vertical position for each curve is offset and is approximately zero at the intercept of the vertical axis at 7705 eV since the background has been subtracted.

Co_3O_4 and Fe_3O_4 consist of a mixture of +2 and +3 valence sites. Some of the edge structure is similar for each of the materials, but there are clear differences in the positions and amplitudes of the various features. A strong pre-edge peak exists for the Y-Ba-Cu-O sample at 7709 eV for example, but is absent, or very weak and shifted, in the standards. For Co, the shift of the half-height position of the edge is about 1.8 eV from CoO (+2) to Co_3O_4

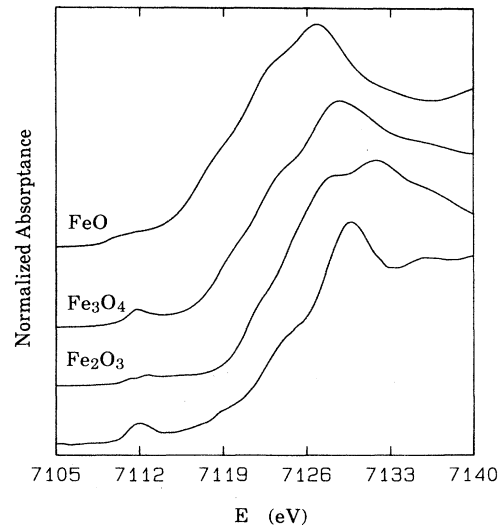

FIG. 13. The Fe near-edge spectra of (from top to bottom) FeO, Fe_3O_4, Fe_2O_3, and Y-Ba-Cu-O($Fe_{0.17}$). The vertical scale for each curve is normalized to give the same step height. The vertical position for each curve is offset and is approximately zero at the intercept of the vertical axis at 7105 eV since the background has been subtracted.

(formal valence =2.67). The Y-Ba-Cu-O($Co_{0.17}$) edge position is very close to that of Co_3O_4, suggesting an effective valence between 2.5 and 3 for the Co in Y-Ba-Cu-O.

For the Fe-oxide references, the half-height-edge position increases linearly with the valence from the +2 material (FeO; E_0=7119.7 eV) to the +3 material (Fe_2O_3; E_0=7223.6 eV). The position of the Fe edge for the Y-Ba-Cu-O($Fe_{0.17}$) material is about 7124.3 eV, slightly above the edge position for the +3 material, suggesting that most of the Fe have a valence of +3. For the Y-Ba-Cu-O($Fe_{0.17}$) sample there is also a somewhat sharper rise at the high-energy part of the edge. This, together with the overall shift of the edge to higher energy, may be indicative of an Fe^{4+} valence. We note that extrapolating the linear increase of edge position with valence observed in the standards to a Fe^{4+} valence suggests an edge position near 7127.5 eV, very close to the center of the sharp rise in the edge above 7126 eV (see Fig. 13). A definitive statement cannot be made however because of the lack of a +4 standard, the covalent nature of the Fe–O bonds, and the numerous features observed in the edge which vary significantly. The lower-energy section of the Y-Ba-Cu-O(Fe) edge is qualitatively similar to the Fe_3O_4 data; both have a pre-edge peak at 7112 eV that is much larger than the corresponding feature for the +2 and +3 standards. This would suggest that there are a mixture of +2, +3, and +4 valence states for Fe in Y-Ba-Cu-O.

Lastly, in Fig. 14, we show the change in the Cu K edge between normal Y-Ba-Cu-O and the highly Co-doped sample Y-Ba-Cu-O($Co_{0.3}$) in which the remaining Cu are primarily on the Cu(2) site. Again the edge positions are measured relative to Cu foil data collected at the same time. In this figure we have normalized the data to both the low-energy part of the edge as well as above the edge in the range 9010 to 9020 eV. The main difference in the Cu near-edge data for the Co-doped sample is a sharpening of the high-energy part of the edge and a change in the structure just above the edge. The overall edge position is essentially unshifted, indicating that either the formal valence of the Cu(1) and Cu(2) sites are very similar or, in these strongly covalent materials, the edge position is insensitive to the formal Cu valence. These data indicate that it may be difficult to extract definitive results about the Cu valence from studies of the edge position.

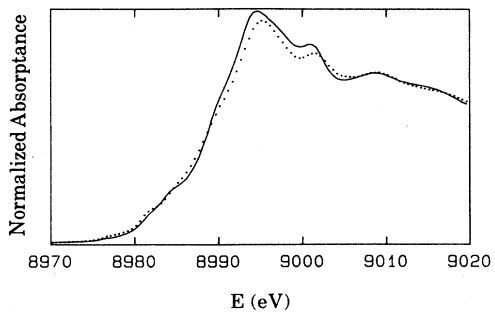

FIG. 14. The Cu near-edge spectra for normal Y-Ba-Cu-O (dotted line) and Y-Ba-Cu-O($Co_{0.3}$) (solid line). The vertical scale for the Y-Ba-Cu-O($Co_{0.3}$) curve is normalized to give the same height at the foot of the step (8985 eV) and above the step (9010 to 9020 eV). The Co-doped sample has a sharper Cu edge from 8987 to 8994 eV.

VII. COMPARISONS WITH OTHER DATA

Neutron studies of Co-substituted samples[18,24,36] agree that Co preferentially occupies the Cu(1) site, although there is some disagreement as to how much Co is on the Cu(2) site. Our results suggest that a small fraction (5%–20%) of the Co is on the Cu(2) site for the highest concentration sample, but no Cu(2) site occupation is needed to fit the two lower concentration samples. The XAFS results thereby indicate that the Co occupation on the Cu(2) plane sites is $<10\%$ for the low-concentration samples. The occupation of Cu(2) sites at the higher concentrations may be sample preparation dependent. These XAFS results are in reasonable agreement with the anomalous x-ray scattering results of Howland *et al.*,[62] who find that the Cu(2) occupation by Co and Fe varies from $\sim 0\%$ at $x \approx 0.07$ to $\sim 20\%$ at $x \approx 0.17$.

A more interesting result from two of the neutron studies[24,36] at high-Co concentration, is that a better refinement is obtained using a less symmetric position of the O(1) [or O(5) as defined in Fig. 1] atoms. Both groups assumed that the O(1) sites were at $(\frac{1}{2},y,0)$, and allowed y to vary. Their refinements yielded a value for this displacement from the normal site position [along a (010) direction] of 0.3 Å, i.e., y=0.08. This clearly indicates distortion within the Co(1) plane similar to the results presented here; the magnitude of the displacement is comparable to the displacement predicted from the chain models ($\pm 0.15, \pm 0.15, 0$) Å. It would be interesting to see whether or not a refinement using our chain parameters would improve the fit. We also note that the temperature parameter for Co(1) and O(1) in these studies is very large, consistent with disorder on the Cu(1) sites.

Neutron magnetic scattering measurements[24] indicate that the magnetic moment on the Co atoms is much less than that of the Cu atoms in the Cu(2) planes. This small average moment is attributed to a large disorder in the directions of the Co moments; it is quite likely that the structural distortion proposed here would contribute significantly to such disorder. Overall, the neutron results suggest that disorder exists in the plane containing the Co(1) sites but are not as specific as the XAFS results.

Some workers[36] have suggested that in the highly doped Co samples, the high-O concentration results in the formation of peroxide ions $(O_2)^{2-}$. If a peroxide ion replaced several of the O(1) atoms near a Co atom, then the number of neighboring O would be considerably greater than 5. We see no evidence for such a direct substitution of O by $(O_2)^{2-}$. However, the distortions in the double-chain model do move O atoms together—perhaps two neighboring O(1) atoms could form a peroxidelike structure and thus introduce holes into the Co(1)-O layer.

Many of the recent papers on Fe-substituted Y-Ba-Cu-O focus on Mössbauer measurements. In all cases the Fe is found to be primarily on the Cu(1) site. Several peaks are observed in the Mössbauer spectra; usually one peak is

attributed to the Cu(2) site and the rest to the Cu(1) site. Most analyses use at least four quadrupole doublets to fit the data and one decomposed the structure into six doublets,[42] corresponding to six inequivalent sites. The crucial point here is that none of these investigations assumed off-center displacements of the Fe atoms—the different Cu(1) sites are usually assumed to correspond to different O coordinations and/or to a mixture of +3 and +4 valences. The large displacements for some of the Fe atoms, obtained from the XAFS analysis, would certainly contribute to the observed quadrupole splittings and for some of these strongly covalent bonds might play a major role.

Additional evidence for structural disorder in Y-Ba-Cu-O(Fe) is obtained in a combined x-ray and neutron-diffraction investigation of a lightly Fe-substituted sample.[61] As for the Co samples, a large thermal parameter for the O(1) site is obtained even at low temperatures.

Two additional XAFS studies[63,64] on Fe-substituted materials have been reported. One[63] is on a highly O-depleted Y-Ba-Cu-O(Fe) sample, where the Fe is found to have ~2.8 O neighbors at 1.93 Å. This value is surprisingly long for an Fe atom on the Cu(1) site if the O(1) atoms are missing. It is not clear whether or not the 1.93-Å distance we obtain when we use a 3-Gaussian fit to the Fe-O peak actually corresponds to the c-axis distance reported for this O-depleted sample. The second study[64] examined several concentrations of Fe-substituted Y-Ba-Cu-O. They concluded that only a double-distance fit, with Fe-O distances of 1.84 and 1.94 Å, were reasonable and consistent. These distances agree with our constrained, two Gaussian fits to the Fe-O environment. However, as discussed in Sec. V, a significantly improved fit is obtained if we use instead a long (2.36 Å) and a short (1.84–1.88 Å) distance. These distances correspond to the distorted structure proposed for the Co samples and provide an explanation for the low amplitude of the second-neighbor peak. Yang *et al.*[64] apparently did not consider the possibility of distorted sites. They do suggest that a clustering of Fe-O-Fe-O-Fe may exist along the b axis.

Yang *et al.*[64] have also studied the near-edge structure of Fe in Y-Ba-Cu-O. Their analysis indicates that the Fe is mainly +3, but small amounts of Fe^{+2} and/or Fe^{+4} may be present. These results are consistent with our determination of a mixture of +2, +3, and +4 valence states for Fe, with a predominance of Fe^{+3}.

Finally, we consider the question—why does the substitution of Co (or Fe) at very low concentrations ($<2\%$) change the macroscopic structure from orthorhombic to tetragonal with relatively little change in T_c, while somewhat higher dopant concentrations [still a relatively small fraction of the Cu(1) sites substituted] depress T_c with a nearly linear concentration dependence?[14] The answer may lie in the aggregation of the Co atoms into distorted zigzag chains, or some similar structure. Assuming that the Co chains are not superconducting, we expect that at moderate concentrations, percolation will occur and a Co chain will extend entirely across the sample, thereby suppressing superconductivity in the Cu(1) layer. For example, at 6% substitution [18% on the Cu(1) chains], there is enough Co present to form a complete diagonal chain (18 atoms) across a 10×10 atom square. For long chains, the Co concentration required is much less; the percolation threshold will clearly depend critically on the average length of the chains. As discussed above, moderately long chains could promote microscopic twinning at very low concentrations (below the percolation threshold) leading to the tetragonal structure, but leaving most of the layer undistorted. If percolation were the main T_c suppression mechanism, we would expect that T_c should remain high until the percolation threshold was approached and then drop to zero, in contrast to the experimental results.[14]

We think a more important aspect of the zigzag chains is the distortion they introduce into the lattice, a distortion that likely extends a distance away comparable to the length of the chains. These distortions have at least two effects. First the disorder within the Cu(1) layer modifies the overlap of the Cu and O orbitals. This may reduce the electron-electron coupling within the layer thereby making the Cu(1)-O layer a poorer superconductor. Second, the distorted Co(1) [and O(1)] sites will also change the coupling between the Cu(1) and Cu(2) layers through small changes in the positions of the O(4) and the Ba atoms. We think this static structural disorder in the Cu(1) layer plays a major role in modifying the electronic structure and is more important that the transition, observed on a macroscopic scale, from orthorhombic to tetragonal symmetry.

An important competing charge transfer effect is the change in the number of holes in the Cu(2) layer as a result of the difference in valence between Cu and Co (or Fe), plus the increased O content. Unfortunately, without more accurate measurements of both the O content and the relative fractions of Co^{2+}, Co^{3+}, Fe^{2+}, Fe^{3+}, and Fe^{4+}, it is not possible to make reliable calculations of the resulting change in the hole concentration.

VIII. CONCLUSIONS

Our detailed XAFS study of Co-doped Y-Ba-Cu-O indicates that the Co primarily replaces the Cu(1) atoms, in agreement with earlier investigations. However, the near-neighbor O peak is composed of ~3.5 O atoms at 1.8 Å and ~1.3 O atoms at 2.4 Å, which means that both long and short bonds must be present within the plane containing the Cu(1) sites. The Co second-neighbor peak is unexpectedly low in amplitude, but has considerable structure that is inconsistent with a simple Gaussian broadening of the expected Co-Ba and Co-Cu(Co) bond distances. Measurements of the Cu environment in the highly doped $Co_{0.3}$ sample show a well-defined second-neighbor peak composed of a (larger than in normal Y-Ba-Cu-O) Co-Y peak, two Co-Ba peaks of unequal amplitude, plus the Co-Cu(Co) contribution. These results indicate that most of the remaining Cu in the Y-Ba-Cu-O($Co_{0.3}$) sample is on the Cu(2) site, and that, viewed from the Cu(2) site, the Y, Ba, and Cu(Co) atoms are at their expected distances. The amplitudes are consistent with a small amount of Co (~11% best fit, 5%–20%

reasonable fits) on the Cu(2) site in this highly doped sample. The most important point of this analysis is that the Ba atom positions are *not* strongly *disordered,* and therefore cannot account for the small second-neighbor amplitude observed for the Co *K*-edge data. Therefore, some of the Co atoms must be *displaced considerably* from the normal Cu(1) site, resulting in several different Co-Ba distances. The interference of these Co-Ba peaks produces the small overall second-neighbor peak amplitude.

We propose a simple local structure model that can account for the different Co—O bond lengths in the Cu(1) plane, provides a good fit to the Co second-neighbor peak for the low concentration data, and suggest an explanation for the apparent tetragonal structure of the Co-doped samples. Zigzag chains of three-Co-atom segments can be formed along the ⟨110⟩ direction, that (i) have Co-Co distances that are shorter than the usual Cu-Cu planer distance, (ii) provide a combination of long and short Co—O bonds as are observed in the first-neighbor peak, (iii) provide a good fit and a simple explanation for the reduced amplitude of the second-neighbor Co multipeak structure [some of the Co(1) atoms have an off-center displacement], (iv) have an increased number of O atoms [one additional O for every two Co in the single-chain model of Fig. 9(a)] and (v) fit easily into the square lattice obtained using the lattice constant from diffraction experiments. In this model, some of the O(5) sites near a Co atom are occupied; consequently, linear Cu-O chains can leave the zigzag chain in either the x or the y direction. We think this promotes twining on a microscopic scale[21,65] and thus leads to the observed tetragonal structure. Even at very low concentrations, a tendency for Co to aggregate into chains would lead to a tetragonal component[43] in the crystal structure.

The data for the Fe-doped samples are very similar to the Co substituted samples suggesting a distorted site for the Fe atoms also. However, there appears to be a nonnegligible fraction of the Fe on the Cu(2) site, even at the lower concentrations, which makes detailed modeling inappropriate. The small, second-neighbor peak clearly indicates that the second-neighbor Fe-X distances are badly disordered. We think this is a result of an off-center displacement of some of the Fe on the Cu sites. Consequently, the Fe(1) sites are not equivalent to the Cu(1) sites. This feature must be taken into account in assigning the various quadrupole splittings, observed in the Mössbauer data, to specific structures.

A few experiments have hinted at the distortions discussed here.[21,24,36,61] Neutron scattering measurements on Co-substituted samples indicate that both magnetic and structural disorder exist within the plane containing the Co(1) atoms. An electron-diffraction study of Fe-doped material has indicated chains of dopant atoms along the ⟨110⟩ directions. The large thermal parameters observed for the Co(1) and O(1) atoms in the neutron measurements can be understood in terms of the displaced atoms of the chain models proposed here.

The position of the Co edge in the substituted Y-Ba-Cu-O samples is very close to that of Co_3O_4 suggesting that the valence of Co in Y-Ba-Cu-O is between 2.5 and 3; in addition, the structure in the lower part of the near edge is also quite similar to that in Co_3O_4. Consequently, it is likely that the valence of Co is a mixture of +2 and +3. For the Fe-substituted samples, the average position of the edge corresponds to a valence slightly greater than 3. However, an additional step in the high-energy part of the edge is consistent with the presence of some Fe^{4+}, suggesting a mixture of valences. Finally, a comparison of the Cu near-edge results for normal Y-Ba-Cu-O and highly Co-substituted material [mostly Cu(2) remaining] shows essentially no shift in the edge, suggesting that the formal valence of the Cu(1) and Cu(2) sites is the same, or possibly that, in this highly covalent material, the *K* edge is relatively insensitive to the valence.

We think that the observed structural distortions, induced by Co or Fe substitution, play an important role in the suppression of T_c by changing the electron-electron coupling within the Cu(1) layer and also the coupling between the Cu(2) planes and the Cu(1) layers. We suggest that these distortions are more important that the orthorhombic-to-tetragonal transition.

Note added in proof. Miceli *et al.* [Phys. Rev. B **38**, 9209 (1988)] found that Co substitution enhances the antiferromagnetic coupling between chain and plane Cu sites, in contrast to Ref. 24. The magnetic properties of substituted Co may be sample dependent.

ACKNOWLEDGMENTS

We would like to thank R. S. Howland for assistance in the early stages of the analysis. The experiments were performed at Stanford Synchrotron Radiation Laboratory, which is funded by the Department of Energy under Contract No. DE-AC03-82-ER-13000, Office of Basic Energy Sciences, Division of Chemical Sciences, and the National Institutes of Health, Biotechnology Resource Program, Division of Research Resources. This research was supported in part by National Science Foundation Grant No. DMR 85-05549 and the Swedish Natural Science Research Council.

[1]R. J. Cava, B. Batlogg, R. B. van Dover, D. W. Murphy, S. Sunshine, T. Siegrist, J. P. Remeika, E. A. Rietman, S. Zahurak, and G. P. Espinosa, Phys. Rev. Lett. **58**, 1676 (1987).

[2]M. A. Beno, L. Soderholm, D. W. Capone II, D. G. Hinks, J. D. Jorgensen, J. D. Grace, I. K. Schuller, C. U. Segre, and K. Zhang, Appl. Phys. Lett. **51**, 57 (1987).

[3]T. Siegrist, S. Sunshine, D. W. Murphy, R. J. Cava, and S. M. Zahurak, Phys. Rev. B **35**, 7137 (1987).

[4]R. M. Hazen, L. W. Finger, R. J. Angel, C. T. Prewitt, N. L. Ross, H. K. Mao, C. G. Hadidiacos, P. H. Hor, R. L. Meng, and C. W. Chu, Phys. Rev. B **35**, 7238 (1987).

[5]P. M. Grant, R. B. Beyers, E. M. Engler, G. Lim, S. S. P. Parkin, M. L. Ramirez, V. Y. Lee, A. Nazzal, J. E. Vazquez, and

R. J. Savoy, Phys. Rev. B **35**, 7242 (1987).
[6]Y. LePage, W. R. McKinnon, J. M. Tarascon, L. H. Greene, G. W. Hull, and D. M. Hwang, Phys. Rev. B **35**, 7245 (1987).
[7]J. D. Jorgensen, M. A. Beno, D. G. Hinks, L. Soderholm, K. J. Volin, R. L. Hitterman, J. D. Grace, I. K. Shuller, C. U. Segre, K. Zhang, and M. S. Kleefisch, Phys. Rev. B **36**, 3608 (1987).
[8]C. C. Torardi, E. M. McCarron, P. E. Bierstedt, A. W. Sleight, and D. E. Cox, Solid State Commun. **64**, 497 (1987).
[9]J. D. Jorgensen, B. W. Veal, W. K. Kwok, G. W. Crabtree, A. Umezawa, L. J. Nowicki, and A. P. Paulikas, Phys. Rev. B **36**, 5731 (1987).
[10]P. Marsh, T. Siegrist, R. M. Fleming, L. F. Schneemeyer, and J. V. Waszczak, Phys. Rev. B **38**, 874 (1988).
[11]R. Fleming, P. Marsh, R. J. Cava, and J. J. Krajewski, Phys. Rev. B **38**, 7026 (1988).
[12]Y. Maeno, M. Kato, Y. Aoki, and T. Fujita, Jpn. J. Appl. Phys. **26**, L1982 (1987).
[13]Y. Maeno, T. Tomita, M. Kyogoku, S. Awaji, Y. Aoki, K. Hoshino, A. Minami, and T. Fujita, Nature (London) **328**, 512 (1987).
[14]J. M. Tarascon, P. Barboux, P. F. Miceli, L. H. Greene, G. W. Hull, M. Eibschutz, and S. A. Sunshine, Phys. Rev. B **37**, 7458 (1988).
[15]J. M. Tarascon, P. Barboux, B. G. Bagley, L. H. Greene, W. R. McKinnon, and G. W. Hull, in *Chemistry of High-Temperature Superconductors,* ACS Symposium Series, No. 351, edited by D. L. Nelson, M. S. Whittingham, and T. F. George (American Chemical Society, Washington, DC, 1987), p. 198.
[16]G. Gonzalez, D. Rios-Jara, T. Akachi, R. Barrio, L. Banos, and R. Escudero, Mater. Res. Soc. Symp. Proc. **99**, 899 (1988).
[17]M. Mehbod, P. Wyder, R. Deltour, Ph. Duvigneaud, and G. Naessens, Phys. Rev. B **36**, 8819 (1987).
[18]P. F. Miceli, J. M. Tarascon, L. H. Greene, P. Barboux, F. J. Rotella, and J. D. Jorgensen, Phys. Rev. B **37**, 5932 (1987).
[19]J. M. Tarascon, P. Barboux, L. H. Greene, G. W. Hull, and B. G. Bagley, Mater. Res. Soc. Symp. Proc. **99**, 523 (1988).
[20]J. M. Tarascon, L. H. Greene, P. Barboux, W. R. McKinnon, G. W. Hull, T. P. Orlando, K. A. Delin, S. Foner, and E. J. McNiff, Jr., Phys. Rev. B **36**, 8393 (1987).
[21]P. Bordet, J. L. Hodeau, P. Strobel, M. Marezio, and A. Santoro, Solid State Commun. **66**, 435 (1988); J. Hodeau, P. Bordet, J. Capponi, C. Chaillout, and M. Marezio, Physica C **153–155**, 582 (1988).
[22]S. X. Dou, A. J. Bourdillon, X. Y. Sun, J. P. Zhou, H. K. Liu, N. Savvides, D. Haneman, C. C. Sorrell, and K. E. Easterling, J. Phys. C **21**, L127 (1988).
[23]I. Sankawa, M. Sato, and T. Konaka, Jpn. J. Appl. Phys. **27**, L28 (1988).
[24]P. Zolliker, D. E. Cox, J. M. Tranquada, and G. Shirane, Phys. Rev. B **38**, 6575 (1988).
[25]M. F. Yan, W. W. Rhodes, and P. K. Gallagher, J. Appl. Phys. **63** 821 (1988).
[26]I. Felner, I. Nowik, and Y. Yeshurun, Phys. Rev. B **36**, 3923 (1987).
[27]U. S. Brahme, G. Kordas, and R. J. Kirkpatrick, Mater. Res. Soc. Symp. Proc. **99**, 809 (1988).
[28]G. Xiao, M. Z. Cieplak, D. Musser, A. Gavrin, F. H. Streitz, C. L. Chien, J. J. Rhyne, and J. A. Gotaas, Nature (London) (to be published).
[29]G. Xiao, M. Z. Cieplak, A. Gavrin, F. H. Streitz, A. Bakhshai, and C. L. Chien, Mater. Res. Soc. Symp. Proc. **99**, 399 (1988).
[30]B. Jayaram, S. K. Agarwal, C. V. Rao, and A. V. Narlikar, Phys. Rev. B **38**, 2903 (1988).
[31]T. Takabatake and M. Ishikawa, Solid State Commun. **66**, 413 (1988).
[32]S. B. Oseroff, D. C. Vier, J. F. Smyth, C. T. Salling, S. Schultz, Y. Dalichaouch, B. W. Lee, M. B. Maple, Z. Fisk, J. D. Thompson, J. L. Smith, and E. Zirngiebl, Solid State Commun. **64**, 241 (1987).
[33]C. Jee, D. Nichols, J. Ciasullo, J. E. Crow, T. Mihalisin, G. N. Myer, M. V. Kuric, S. H. Bloom, and R. P. Guertin, Mater. Res. Soc. Symp. Proc. **99**, 769 (1988).
[34]R. C. Sherwood, S. Jin, T. H. Tiefel, R. B. van Dover, R. A. Fastnacht, M. F. Yan, and W. W. Rhodes, Mater. Res. Soc. Symp. Proc. **99**, 503 (1988).
[35]S. Horn, K. Reilly, Z. Fisk, R. S. Kwok, J. D. Thompson, H. A. Borges, C. L. Chang, and M. L. den Boer, Phys. Rev. B **38**, 2930 (1988).
[36]Y. K. Tao, J. S. Swinnea, A. Manthiram, J. S. Kim, J. B. Goodenough, and H. Steinfink, J. Mater. Res. **3**, 248 (1988); Mater. Res. Soc. Symp. Proc. **99**, 519, (1988).
[37]J. F. Bringley, T.-M. Chen, B. A. Averill, K. M. Wong, and S. J. Poon, Phys. Rev. B **38**, 2432 (1988).
[38]R. Gomez, S. Aburto, M. L. Marquina, M. Jimenez, V. Marquina, C. Quintanar, T. Akachi, R. Escudero, R. A. Barrio, and D. Rios-Jara, Phys. Rev. B **36**, 7726 (1987).
[39]C. W. Kimball, J. L. Matykiewicz, J. Giapintzakis, A. E. Dwight, M. B. Brodsky, M. Slaski, B. D. Dunlap, and F. Y. Fradin, Physica B **148**, 309 (1987).
[40]T. J. Kistenmacher, W. A. Bryden, J. S. Morgan, K. Moorjani, Y-w. Du, Z. Q. Qiu, H. Tang, and J. C. Walker, Phys. Rev. B **36**, 8877 (1987).
[41]H. Tang, Z. Q. Qiu, Y-w. Du, G. Xiao, C. L. Chien, and J. C. Walker, Phys. Rev. B **36**, 4018 (1987).
[42]I. Nowik, M. Kowitt, I. Felner, and E. R. Bauminger, Phys. Rev. B **38**, 6677 (1988).
[43]M. Eibschutz, M. E. Lines, J. M. Tarascon, and P. Barboux, Phys. Rev. B **36**, 2896 (1988).
[44]C. Blue, K. Elgaid, I. Zitkovsky, P. Boolchand, D. McDaniel, W. C. H. Joiner, J. Oostens, and W. Huff, Phys. Rev. B **37**, 5905 (1988).
[45]C. W. Kimball, J. L. Matykiewicz, J. Giapintzakis, H. Lee, B. D. Dunlap, M. Slaski, F. Y. Fradin, C. Segre, and J. D. Jorgensen, Mater. Res. Soc. Symp. Proc. **99**, 107 (1988).
[46]E. R. Bauminger, M. Kowitt, I. Felner, and I. Nowik, Solid State Commun. **65**, 123 (1988).
[47]T. Tamaki, T. Komai, A. Ito, Y. Maeno, and T. Fujita, Solid State Commun. **65**, 43 (1988).
[48]Q. A. Pankhurst, A. H. Morrish, and X. Z. Xhou, Phys. Lett. A **127**, 231 (1988).
[49]X. Z. Zhou, M. Raudsepp, Q. A. Pankhurst, A. H. Morrish, Y. L. Luo, and I. Maartense, Phys. Rev. B **36**, 7230 (1987).
[50]T. M. Hayes and J. B. Boyce, in *Solid State Physics,* edited by H. Ehrenreich, F. Seitz, and D. Turnbull (Academic, New York, 1982), Vol. 37, p. 173.
[51]E. A. Stern and S. M. Heald, in *Handbook on Synchrotron Radiation,* edited by E. E. Koch (North-Holland, New York, 1983), Vol. 1, p. 955.
[52]F. Bridges, J. B. Boyce, T. Claeson, T. H. Geballe, and J. M. Tarascon, in *Synchrotron Radiation in Materials Research,* edited by J. Weaver, J. Gland, and R. Clarke (Materials Research Society, Pittsburgh, in press).
[53]J. B. Boyce, F. Bridges, T. Claeson, and T. H. Geballe, in

XAFS V—Proceedings of the Fifth International Conference on X-Ray Absorption Fine Structure, edited by E. A. Stern (Elsevier, Amsterdam, in press).

[54]J. B. Boyce, F. Bridges, T. Claeson, T. H. Geballe, M. Nygren, and J. M. Tarascon, in *Towards the Theoretical Understanding of High Temperature Superconductors,* edited by S. Lundqvist, E. Tosatti, M. Tosi, and Yu Lu (World Scientific, Singapore, 1988), p. 617.

[55]J. B. Boyce, F. Bridges, T. Claeson, R. S. Howland, T. H. Geballe, and M. Nuygren, Physica C **153–155**, 852 (1988).

[56]J. B. Boyce, F. Bridges, T. Claeson, and T. H. Gabelle, Phys. Scr. **37**, 912 (1988).

[57]F. Bridges, Nucl. Instrum. Methods Phys. Res. Sect. A **257**, 447 (1987).

[58]J. B. Boyce, F. Bridges, T. Claeson, and M. Nygren, Phys. Rev. B **39**, 6555 (1989).

[59]A. G. McKale, B. W. Veal, A. P. Paulikas, S.-K. Chan, and G. S. Knapp, J. Am. Chem. Soc. **110**, 3763 (1988).

[60]P. Miceli (private communication).

[61]G. Roth, G. Heger, B. Renker, J. Pannetier, V. Caignaert, M. Hervieu, and B. Raveau, Physica C **153–155**, 972 (1988).

[62]R. S. Howland, T. H. Geballe, S. S. Laderman, A. Fischer-Colbrie, M. Scott, J. M. Tarascon, and P. Barboux (unpublished).

[63]K. Donnelly, J. M. D. Coey, S. Tomlinson, and J. M. Greneche (unpublished).

[64]C. Y. Yang, S. M. Heald, J. M. Tranquada, Y. Xu, Y. L. Wang, A. R. Moodenbaugh, D. W. Welch, and M. Suenaga (unpublished).

[65]X. Youwen, A. Moodenbaugh, R. Sabatini, and M. Suenaga, in *Proceedings of the Symposium on High-Temperature Superconductors II,* edited by D. Capone II, W. H. Butler, B. Batlogg, and C. W. Chu (Materials Research Society, Pittsburgh, 1988), Vol. EA-14, p. 373.